Magnetism of the Kondo compound CeAuAl

1997 J. Phys.: Condens. Matter 9 4743

(http://iopscience.iop.org/0953-8984/9/22/024)

J. Phys.: Condens. Matter **9** (1997) 4743–4753. Printed in the UK PII: S0953-8984(97)81989-3

Magnetism of the Kondo compound CeAuAl

D T Adroja†, B D Rainford†, Latika Menon‡ and S K Malik‡

† Department of Physics, Southampton University, Southampton SO17 1BJ, UK
‡ Tata Institute of Fundamental Research, Bombay, 400 005, India

Received 19 February 1997, in final form 3 April 1997

Abstract. The magnetism of the Kondo lattice compound CeAuAl has been investigated through neutron scattering, magnetoresistance, transport and magnetic measurements. Neutron diffraction at 1.5 K revealed a modulated antiferromagnetic structure. Inelastic neutron scattering spectra showed two well defined crystal-field excitations at 24.2 meV and 45.8 meV. The crystal-field parameters have been estimated from an analysis of the neutron spectra and susceptibility data. An estimate of the Kondo temperature has been made by comparison of the low-temperature negative magnetoresistance with Schlottmann's scaling form for the $J = \frac{1}{2}$ Kondo impurity. An analysis of thermoelectric power data has been made on the basis of Fischer's theory, which allows Kondo and crystal-field effects to be taken into account.

1. Introduction

In recent years experimental investigations on the ternary equiatomic compounds of type CeTX (T = transition metal and X = metalloid) have attracted considerable attention due to the range of unusual ground states which they possess. They include hybridization gap insulators ('Kondo insulators') like CeNiSn and CeRhSb [1, 2] and ferromagnetic Kondo lattices [3], as well as Kondo lattices exhibiting the more usual properties such as magnetic ordering with reduced moments [4]. Crystallographic and magnetic studies of CeTAl compounds, with T = Cu, Ni, Pd, Pt and Au, have been reported recently [5–8]. The compounds with T = Au and Pt crystallize in the orthorhombic ϵ-TiNiSi-type structure (space group $Pnma$), while those with T = Cu, Ni and Pd have the hexagonal ZrNiAl-type structure (space group $P\bar{6}2m$). The magnetic susceptibility of CeAuAl and CePtAl exhibits a Curie–Weiss behaviour in the high-temperature regime with an effective magnetic moment close to $2.54\mu_B$, indicating that the Ce ions are close to a stable trivalent state. The susceptibility of CeNiAl and CeCuAl shows a weak temperature-dependent behaviour indicating an intermediate-valence state for the Ce ions [6, 7].

We have been investigating CeTX compounds through neutron scattering, thermoelectric power and high-field magnetoresistance measurements [9–11]. Our aim has been to attempt a synthesis, as far as possible, in our understanding of the magnetic and transport properties in the incoherent Kondo regime, where single-ion Kondo theory should obtain. A key element in this endeavour is a detailed knowledge of the crystal-field wavefunctions and the dynamical susceptibility, which can be deduced from inelastic neutron scattering measurements. In the present paper we concentrate on CeAuAl which magnetization and transport measurements identify as an antiferromagnetic Kondo lattice compound [8]. Our inelastic neutron scattering studies of this compound show the presence of two well defined crystal-field excitations at 24.2 meV and 45.8 meV. Evidence of an

0953-8984/97/224743+11$19.50

incommensurably modulated magnetic structure has come from a neutron diffraction study at low temperatures. The Kondo temperature $T_K \sim 3.6$ K has been estimated from an analysis of magnetoresistance results on the basis of Schlottmann's scaling for a $J = \frac{1}{2}$ Kondo impurity [12]. An analysis of thermoelectric power data for CeAuAl on the basis of a Kondo plus crystal-field model proposed by Fischer [13] shows a good agreement between experiment and theory.

2. Experimental procedure

Polycrystalline samples of CeAuAl were synthesized by arc melting the constituent elements Ce, Au and Al, of purity 99.99% or better, under a high-purity argon atmosphere. Powder x-ray and neutron diffraction were used to check the phase purity. The neutron diffraction measurements were carried out using the D1B diffractometer at ILL Grenoble at 1.5 K and 8 K. The incident neutron wavelength was 2.52 Å. Inelastic neutron scattering measurements were carried out using the HET time-of-flight neutron spectrometer at the ISIS Facility, Rutherford Appleton Laboratory, CLRC, UK. The thermoelectric power was measured using the differential method: Pb wires of 99.999% purity were used as reference junctions, across which the differential voltages (ΔV) were measured. The temperature difference (ΔT) across the sample length was measured using a Au–Fe/chromel thermocouple. The thermopower of the sample was calculated from the slope of the ΔV versus ΔT curve. Magnetoresistance measurements in the temperature range 1.7 K to 14 K were carried out using a four-probe ac technique and steady magnetic fields up to 12 T, with the current flowing parallel to the applied magnetic field.

3. Results and discussion

3.1. X-ray and neutron powder diffraction

The analysis of the room temperature x-ray diffraction data revealed that CeAuAl crystallizes in the orthorhombic ϵ-TiNiSi-type structure with the lattice parameters $a = 7.562(6)$ Å, $b = 4.589(3)$ Å and $c = 7.727(4)$ Å. The numbers in parentheses are the errors in the least-significant digit. The neutron diffraction pattern at 8 K was analysed using the Rietveld procedure on the basis of the *Pnma* space group, with the atoms in the crystallographic 4(c) sites. The lattice parameters and atomic positions obtained by least-squares refinement are $a = 7.560(2)$ Å, $b = 4.581(3)$ Å, $c = 7.650(2)$ Å and $x_{\mathrm{Ce}} = 0.037(4)$, $z_{\mathrm{Ce}} = 0.688(1)$, $x_{\mathrm{Au}} = 0.197(1)$, $z_{\mathrm{Au}} = 0.063(2)$, $x_{\mathrm{Al}} = 0.322(1)$ and $z_{\mathrm{Al}} = 0.412(2)$. A comparison of the lattice parameters at 300 K (obtained from x-ray diffraction) and 8 K (obtained from neutron diffraction) reveals that the lattice parameters a and b remain almost constant, while the lattice parameter c shows a small contraction at low temperatures. The neutron diffraction pattern at 1.5 K showed a number of extra peaks of magnetic origin. A preliminary analysis shows that most of the observed strong magnetic peaks can be indexed assuming a modulated magnetic structure described by a wave vector $\boldsymbol{k} = (0.69, 0, 0)$. The detailed analysis of the magnetic structure is in progress and will be published elsewhere.

3.2. Inelastic neutron scattering

The inelastic neutron scattering measurements were made with 60 meV incident neutrons using the HET time-of-flight spectrometer at ISIS. The sample was cooled to 16 K in a top-loading closed-cycle refrigerator. The spectrum, summed over the two-metre detector

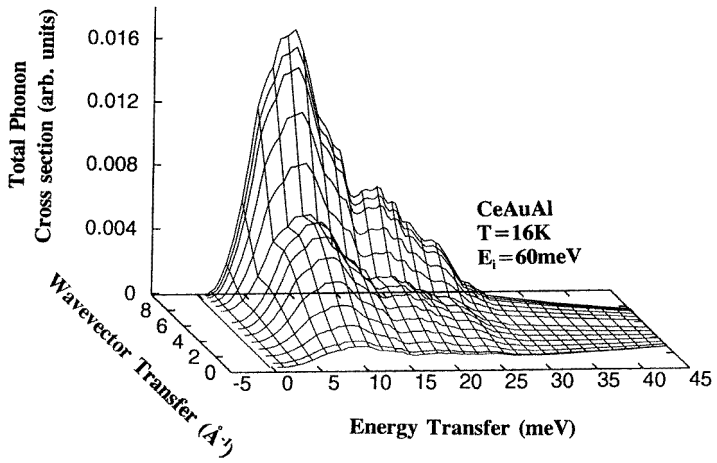

Figure 1. The total phonon cross section of CeAuAl over the entire (Q, ω) grid at 16 K, calculated using the Monte Carlo simulation algorithm (see the text).

bank (scattering angles between 11.5° and 26.5°, with average scattering angle 19°) has two components, namely magnetic scattering from the cerium 4f electrons and phonon scattering. Since the phonon scattering increases with the square of the neutron wavevector transfer, at low scattering angles the phonon cross section is due largely to multiple-scattering processes in which the neutron is scattered more than once in the sample through large angles. The magnetic cross section, on the other hand, decreases with increasing wavevector due to the 4f form factor. In order to separate the magnetic and phonon scattering in the spectrum we have scaled the scattering in the high-angle spectrum (scattering angle 135°), in which the magnetic scattering is negligible. The scaling factor was obtained by calculating the total phonon scattering cross section for CeAuAl over the entire (Q, ω) grid, using a Monte Carlo approach, as suggested by Osborn [14]. The method employs the single-phonon density of states, $Z(\omega)$, as a kernel for the Monte Carlo calculation. This was estimated from the measured high-angle spectrum: at a scattering angle of 135° the phonon scattering is dominated by single-phonon processes, and so the measured cross section, after correction for the population factor, is proportional to $Z(\omega)/\omega$ in the incoherent approximation. The Monte Carlo simulations used the DISCUS program, originally written by Johnson and recently modified by Osborn [14]. The output of the simulations gave the single-phonon scattering cross section, and the multiple scattering up to sixth order, fully corrected for temperature, geometry and absorption. The latter is particularly important for the present experiment because of the absorption cross section of gold.

The total phonon cross section calculated for a flat-plate sample of CeAuAl at 16 K and an incident neutron energy of 60 meV is shown in figure 1 over the whole (Q, ω) range. By taking the ratio of the total cross sections at angles 135° and 19°, we then have a scaling factor which allows us to estimate the phonon scattering in the low-angle bank by scaling the measured scattering in the high-angle bank. Figure 2(a) shows the total scattering (magnetic plus phonon) in the low-angle bank (points), while the histogram represents the estimated total phonon scattering. The points in figure 2(b) show the difference between the two curves in figure 2(a), the resulting spectrum representing the magnetic scattering from CeAuAl. Two well defined inelastic peaks are seen centred at 24.2 meV and 45.8 meV. These arise from crystal-field excitations of the Ce ions. The point symmetry of the Ce^{3+}

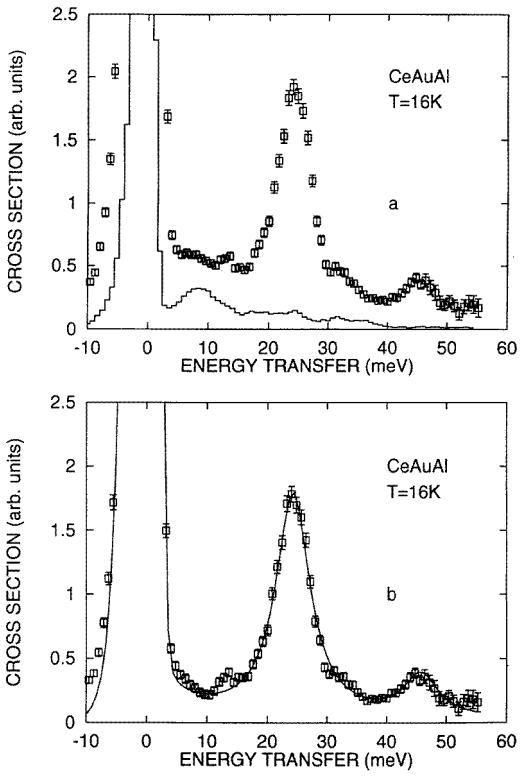

Figure 2. (a) Points: total neutron scattering from CeAuAl in the 2 m detector bank of the HET spectrometer at 16 K for an incident neutron energy of 60 meV. The histogram shows the estimated phonon scattering from scaling high-angle scattering. (b) Magnetic scattering (total scattering minus phonon scattering) for CeAuAl. The solid line represents the fit (see the text).

ions in the orthorhombic ϵ-TiNiSi-type structure of CeAuAl is very low and the ground $J = 5/2$ multiplet splits into three doublets. Only two inelastic excitations are expected in the neutron spectrum at low temperature, corresponding to transitions between the ground state and the first and second excited states of the crystal-field-split multiplet. The small peak near 13 meV (figure 2(b)) is probably a residual feature in the phonon scattering which is not accounted for by the scaling procedure. The latter, after all, depends on the incoherent approximation; while this gives a good representation of the phonon scattering over most of the Q-range, one might expect to see some coherent features at small wavevectors, especially in a sample with a largely coherent cross section.

The linewidth of the inelastic peaks is 3.5 meV which is considerably larger than the instrumental resolution (0.6 meV). This indicates the presence of strong spin–lattice coupling, presumably due to interactions between the 4f electron and the conduction electrons; spin–spin interactions can probably be ruled out since intersite (RKKY) interactions are weak in this compound, as can be judged by the low magnetic ordering temperature (see section 3.3). Analysis of the crystal field using a superposition-model approach [15, 16] shows that for the low point symmetry of the Ce^{3+} ion in CeAuAl the crystal-field (CF) Hamiltonian has three rank-two and five rank-four terms:

$$H_{CF} = B_2^0 O_2^0 + B_2^1 O_2^1 + B_2^2 O_2^2 + B_4^0 O_4^0 + B_4^1 O_4^1 + B_4^2 O_4^2 + B_4^3 O_4^3 + B_4^4 O_4^4. \quad (1)$$

Here the O_n^m are the Stevens operators and the B_n^m are the crystal-field parameters. The second-order CF parameters can be determined accurately from the single-crystal susceptibility. At present single-crystal susceptibility data for CeAuAl are not available, so we are obliged to vary all of the CF parameters independently. Clearly fitting eight CF parameters using the positions and intensities of only two inelastic peaks in the neutron spectrum is a rather underdetermined problem. However, we can be guided by similar Ce compounds for which we have more information. The point symmetry and crystal-field spectrum for CeAuAl are similar to those for CePdSn, and for CePdSn we have previously obtained accurate values of all eight CF parameters from the simultaneous analysis of single-crystal susceptibility and inelastic neutron scattering data [15]. We have therefore used the CF parameters of CePdSn as a starting point in the CF analysis of CeAuAl. The values of the CF parameters obtained from least-squares fits to the neutron spectrum of CeAuAl are: $B_2^0 = 1.42$, $B_2^1 = -3.17$, $B_2^2 = 2.45$, $B_4^0 = 0.02$, $B_4^1 = 0.34$, $B_4^2 = 0.16$, $B_4^3 = 0.05$ and $B_4^4 = -0.04$ (in units of meV). The solid line in figure 2(b) represents the fitted neutron spectrum. The agreement between experimental and calculated results is excellent. However, it is worth stressing that this set of parameters is probably not unique: single-crystal susceptibility data would be a very useful check on the second-order parameters.

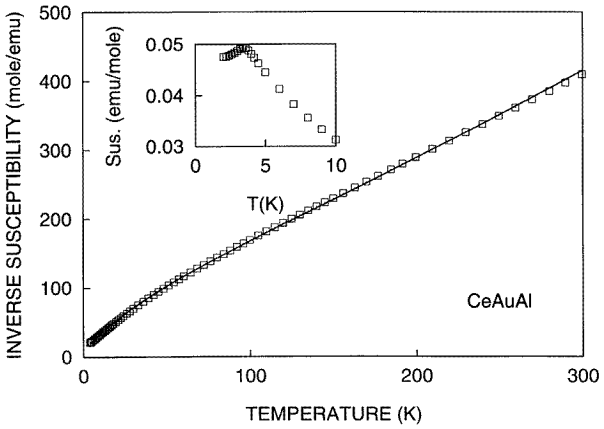

Figure 3. The inverse magnetic susceptibility versus the temperature for CeAuAl; the solid line represents the fit to equation (2) using the crystal parameters (see the text); the inset shows the susceptibility versus the temperature.

3.3. Magnetization

The magnetic susceptibility of CeAuAl exhibits a peak at 3.8 K (see the inset in figure 3), indicating the onset of antiferromagnetic ordering of the Ce moments. In the high-temperature regime the susceptibility exhibits Curie–Weiss behaviour with an effective paramagnetic moment $\mu_{eff} = 2.5\mu_B$ and a paramagnetic Curie temperature $\theta_p = -35$ K. Deviations from Curie–Weiss behaviour are apparent below 50 K. These are attributed to the effect of the CF splitting of the $J = 5/2$ multiplet of the Ce^{3+} ion. The temperature dependence of the susceptibility may be used as an independent check on the CF parameters obtained from the analysis of neutron spectra in section 3.2. To this end the mean-field

susceptibility was written as

$$\chi_M = \frac{\chi_{CF}}{1 - \lambda\chi_{CF}} + \chi_0 \tag{2}$$

where λ is the mean-field constant representing the exchange coupling between the Ce ions and χ_{CF} is the single-ion susceptibility calculated from the crystal-field parameters. A temperature-independent Pauli susceptibility χ_0 was also included. The values obtained from least-squares fitting the susceptibility data to the mean-field expression (2) are $\lambda = -10.45$ mol emu^{-1} and $\chi_0 = -1 \times 10^{-4}$ emu mol^{-1} respectively. The fit is shown as the solid line in figure 3; the good overall agreement gives support to the validity of the CF parameters. The negative sign of χ_0 indicates a small diamagnetic Pauli susceptibility arising from the conduction electrons.

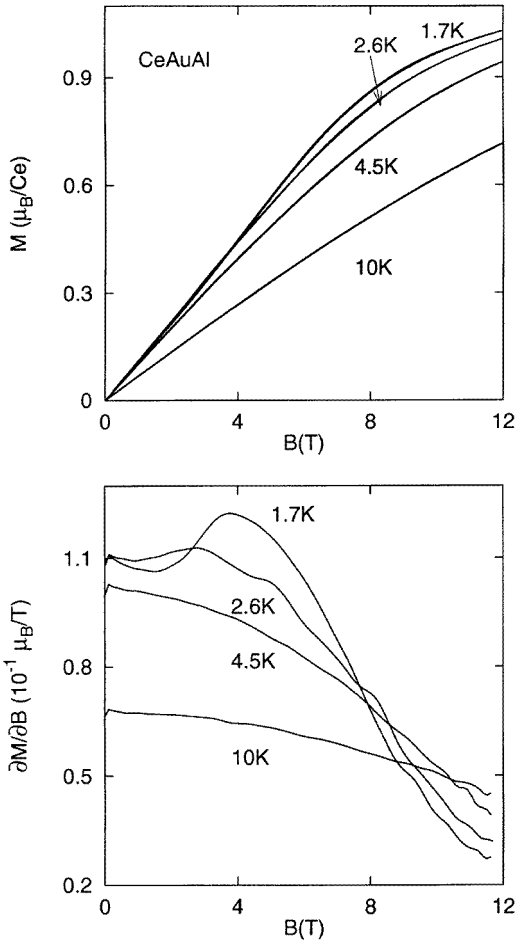

Figure 4. Top: magnetization versus field isotherms for CeAuAl at various temperatures. Bottom: the differential susceptibility, $\partial M/\partial B$, versus B at various temperatures.

Magnetization isotherm measurements were carried out at various temperatures between 1.7 K and 10 K in applied fields up to 12 T (figure 4, top). At 1.7 K the magnetization increases linearly with field up to 2.5 T, but exhibits a slight upward curvature above

this field, followed by a tendency towards saturation at the highest fields. To show this metamagnetic behaviour clearly we have plotted the differential susceptibility, $\partial M/\partial B$, versus B in figure 4 (bottom). At 1.7 K, $\partial M/\partial B$ exhibits a broad peak at a field of 3.8 T. This peak becomes less pronounced at 2.6 K and has disappeared by 4.5 K. This suggests that the metamagnetic transition is associated with the polarization of the antiferromagnetic structure by the applied field below T_N. A rough estimate of the saturation magnetic moment was obtained by extrapolation of an M versus $1/B$ plot to $1/B \rightarrow 0$: we find $\mu_{sat} \approx 1.4\mu_B$ at 1.7 K. This value may be compared to the magnetic moment of the CF ground state: using the above CF parameters we find that the b-axis is the easy direction and that $\langle \mu_b \rangle = g_J \langle J_y \rangle \mu_B = 1.56\mu_B$. Allowing for the uncertainties in the extrapolation the agreement must be regarded as satisfactory.

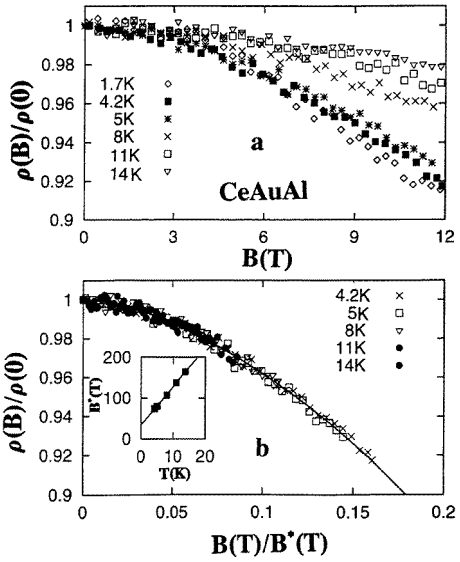

Figure 5. (a) The normalized magnetoresistance, $\rho(B)/\rho(0)$, versus B for CeAuAl at various temperatures. (b) $\rho(B)/\rho(0)$ versus B/B^*, where B^* is the scaling field. The solid line represents Schlottmann's scaling curve for $J = 1/2$. The inset shows B^* versus temperature.

3.4. Magnetoresistance

Figure 5 (top) shows the normalized magnetoresistance, $\rho(B)/\rho(0)$, of CeAuAl for applied fields up to 12 T at various temperatures. At 1.7 K the magnetoresistance decreases with increasing field without any clear sign of the metamagnetism. Between 4.2 K and 14 K the observed magnetoresistance behaviour of CeAuAl is similar to that observed in single-ion Kondo systems. Schlottmann [12] has shown that the magnetoresistance in the Kondo impurity problem can be calculated at zero temperature using Friedel's sum rule, which relates the scattering phase shift of an electron to the occupation number of the corresponding energy levels. By applying the Bethe *ansatz* technique to the Coqblin–Schrieffer Hamiltonian, Schlottmann has obtained exact results for the occupation numbers of Zeeman levels as a function of field for $J = 1/2$ and $J = 1$. For $J \geqslant 3/2$ only an approximate solution is possible, which interpolates between the exact low- and high-field results. Using these results, he has calculated the magnetoresistance of Kondo impurities

for different angular momenta J. His results show that the magnetoresistance exhibits a universal behaviour as a function of the applied field B and temperature T, for a given value of J. This indicates that the underlying physics of the Kondo impurity is dominated by a single energy scale ($g_J\mu B^*$), which is related to the Kondo temperature T_K. The temperature dependence of the scaling field B^* is given by $B^*(T) = B^*(0) + k_BT/g_J\mu$, where the zero-temperature scaling field $B^*(0)$ (called the Kondo field) is related to the Kondo temperature by $T_K = g_J\mu B^*(0)/k_B$. Here g_J and μ are the Landé factor and the magnetic moment of the Kondo ion, respectively.

The first excited CF level in CeAuAl is at 24.2 meV, so at low temperature we can treat each Ce ion as an effective $J = 1/2$ impurity and we can analyse the magnetoresistance data on the basis of Schlottmann's $J = 1/2$ scaling curve (solid line, figure 5, bottom). In this plot the scaling field B^* has been adjusted at each temperature to minimize the deviation between the measured magnetoresistance and the scaling curve for $J = 1/2$. The values of B^* obtained from the analysis are plotted as a function of temperature in the inset of figure 5 (bottom): this shows a linear behaviour, in agreement with the prediction above. The value of the Kondo temperature T_K for CeAuAl, obtained from the slope and intercept of this plot, is 3.6 K.

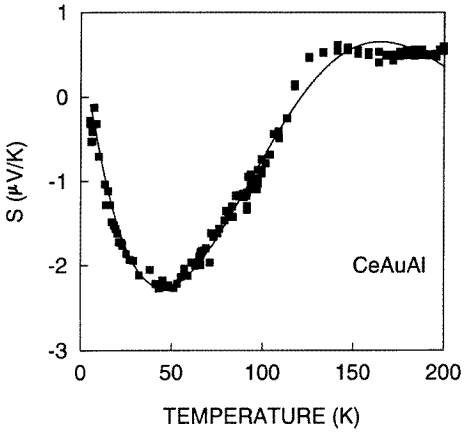

Figure 6. The thermoelectric power versus temperature for CeAuAl; the solid line represents the fit to Fischer's theory (see the text).

3.5. Thermoelectric power

Figure 6 shows the thermoelectric power (TEP) of CeAuAl as a function of temperature. Above 150 K the TEP of CeAuAl is positive and weakly temperature dependent. Below 150 K it changes sign then shows a pronounced minimum at 50 K. The overall 'tilde' shape of the anomaly is similar to that observed in many Ce-based Kondo lattice compounds [9]. This type of behaviour cannot be explained simply by considering the diffusion TEP arising from either electronic or Hall conduction. It is also clear that the temperature scale for the anomaly ($\sim$150 K) is large compared to the Kondo temperature. It would appear that the relevant energy scale is the crystal field, and that the anomaly arises from processes where the conduction electrons scatter inelastically from the Ce ions, causing crystal-field transitions. These processes are frozen out when $k_BT \ll \Delta_{CF}$. It can be shown that the thermopower depends on the integral of $\varepsilon\tau(\varepsilon)(-\partial f/\partial\varepsilon)$ over ε, where $\tau(\varepsilon)$ is the conduction electron's

relaxation time and ε is the electron energy, relative to the Fermi energy. It follows that inelastic scattering processes dominate the thermopower. Peschel and Fulde [17] were the first to consider the thermopower in metals containing magnetic impurities with crystal-field-split energy levels. They found a 'resonance' anomaly in the thermopower in perturbation theory at order J^2V where J and V are the exchange- and spin-independent parts of the sf scattering potential. Fischer [13] has extended this calculation to order J^3V and finds a second contribution arising from the Kondo effect. The total diffusion thermopower may then be written in the form

$$S_d(T) = S_d^{(1)}(T) + S_d^{(2)}(T) + S_d^{latt}(T) \tag{3}$$

where

$$S_d^{(1)} = -A(\pi N(0))^4 J^3 V S_{eff}^2(T) \tag{4}$$

and

$$S_d^{(2)} = -A\frac{\pi}{6}N(0)^3 J^2 V \tilde{S}_f(T). \tag{5}$$

The last term $S_d^{latt}(T)$ is the lattice thermopower, expected for a non-magnetic equivalent of the material being considered, e.g. in the present case LaAuAl. The lattice term is usually small and varies linearly with the temperature. The term $S_d^{(1)}$ above, which is of order J^3V, is the Kondo term, while the $S_d^{(2)}$ term is equivalent to the resonance term calculated by Peschel and Fulde. In cerium alloys which show the Kondo effect, J is negative, so the two terms $S_d^{(1)}$ and $S_d^{(2)}$ have opposite sign. The temperature dependence of the two terms results from the factors

$$S_{eff}^2(T) = \int_{-\infty}^{\infty} \frac{\mathrm{d}\omega}{\pi} \frac{\omega\beta \,\mathrm{Im}\,\chi_f(\omega)}{(\mathrm{e}^{\omega\beta}-1)(1-\mathrm{e}^{\omega\beta})} \tag{6}$$

and

$$\tilde{S}_f(T) = 2\int_0^{\infty} \mathrm{d}\omega \,\mathrm{Im}\,\chi_f^{\perp}(\omega) q(\omega\beta). \tag{7}$$

In equation (7) the factor $q(x)$ is given by

$$q(x) = x\left[1 + \frac{x}{2\pi}\psi'\left(\frac{\mathrm{i}x}{2\pi}\right)\right] \tag{8}$$

where $\psi'(z)$ is the trigamma function. Both factors (6) and (7) involve integrals over the dynamical susceptibility of the f electrons, but the temperature dependence of the integrands is quite different. As a result the total thermopower can change sign as a function of temperature.

Having the thermopower expressed in terms of the dynamical susceptibility is very convenient since we can calculate $\mathrm{Im}\,\chi_f(\omega)$ directly from our model for the crystal field, using the standard RPA result. We find that the temperature dependence of the calculated TEP has the correct form as long as we omit the elastic ('Curie') components of $\mathrm{Im}\,\chi_f(\omega)$: this has the effect of decreasing the magnitude of the $S_d^{(1)}$-term at low temperatures. This is justified by our remark earlier in this section that the thermopower is dominated by inelastic processes. It is likely also that nearly elastic scattering processes will be suppressed at low temperatures by either magnetic order or the onset of coherence due to the translational symmetry of the lattice.

The dynamical susceptibility $\mathrm{Im}\,\chi_f(\omega)$ was calculated from the parameters used to fit the neutron spectrum (figure 2(b)). The two factors (6) and (7) were then calculated as a function of temperature by numerical integration. In calculating the $S_d^{(1)}$-term, we have used

the Suhl–Nagaoka correction for $S_d^{(1)}$ (equation (68) in reference [13]) which introduces the Kondo temperature T_K as an extra parameter [18]. This modifies (4) above by introducing a dividing factor $[\ln^2(T_K/T) + \pi^2 S(S+1)]^{3/2}$. The TEP data were fitted using the form

$$S_d(T) = \frac{a S_{eff}^2(T)}{[\ln^2(T_K/T) + \pi^2 S(S+1)]^{3/2}} + b\tilde{S}_f(T) - \alpha T \tag{9}$$

where αT is a small normal-metallic contribution. The value of the Kondo temperature was kept fixed at $T_K = 3.6$ K during the least-squares fitting. The parameters a, b and α were allowed to vary in order to minimize the deviation between the experimental and calculated TEP. The solid line in figure 6 shows the calculated TEP; $S = 1/2$ was taken for this calculation. The values of a, b and α and obtained from the least-squares fit were 227.2, 0.132 and 0.027 μV K^{-2}). The agreement with the data is quite good, in particular the shape and position of the minimum near 50 K is well fitted.

4. Conclusions

The compound CeAuAl has been characterized using transport, magnetic and neutron scattering measurements. Neutron diffraction measurements reveal an incommensurable magnetic structure at 1.5 K. Inelastic neutron scattering studies show the presence of two well defined crystal-field excitations with an overall splitting of 45.8 meV. The crystal-field parameters have been obtained from the analysis of the neutron spectra. The magnetoresistance shows an excellent scaling with the $J = 1/2$ model of Schlottmann. The Kondo temperature, T_K has been estimated to be 3.6 K from the magnetoresistance scaling. The observed thermoelectric power of CeAuAl shows good agreement with that calculated using Fischer's theory. CeAuAl belongs to the class of Kondo lattice compounds in which the two competing energies, the Kondo energy ($k_B T_K$) and the intersite exchange energy ($k_B T_{RKKY}$) are comparable. It is likely that the magnetic ordering temperature is suppressed by the Kondo interactions.

Acknowledgments

We would like to thank Dr Roger Eccleston (ISIS Facility, Rutherford Appleton Laboratory) for help with the HET measurements and Dr Clemens Ritter (Institut Laue–Langevin, Grenoble) for help with the D1B measurements. Thanks also to Dr Raymond Osborn (Argonne National Laboratory) for providing the programs for the Monte Carlo phonon simulations. This work is supported by grant GR/J 87435 from the UK Engineering and Physical Sciences Research Council.

References

[1] Malik S K and Adroja D T 1991 *Phys. Rev.* B **43** 6277
[2] Takabatake T, Teshima F, Fujii H, Nishigori S, Suzuki T, Fujita T, Tamaguchi Y and Sakurai J 1990 *Phys. Rev.* B **31** 9607
[3] Malik S K and Adroja D T 1991 *Phys. Rev.* B **43** 6296
[4] See, for instance,
Bauer E 1991 *Adv. Phys.* **40** 417
[5] Dönni A, Kitazawa H, Fischer P, Tang J, Kohgi M, Endoh Y and Morii Y 1993 *J. Phys.: Condens. Matter* **7** 1663
Hulliger F 1993 *J. Alloys Compounds* **196** 225
[6] Oesterreicher H 1973 *J. Less-Common Met.* **30** 225

[7] Tuan N C, Sechovsky V, Divis M and Svobada P 1993 *J. Appl. Phys.* **73** 5677
[8] Menon L and Malik S K 1995 *Phys. Rev.* B **51** 5858
[9] Rainford B D, Adroja D T and Geers J M E 1994 *Physica* B **199+200** 556
[10] Rainford B D, Adroja D T, Neville A J and Fort D 1995 *Physica* B **206+207** 209
[11] Adroja D T, Rainford B D and Malik S K 1994 *Physica* B **194–196** 169
[12] Schlottmann P 1983 *Z. Phys.* B **51** 223
[13] Fischer K H 1989 *Z. Phys.* B **76** 315
[14] Johnson M W 1974 DISCUS: a computer program for the calculation of multiple scattering effect in inelastic neutron scattering experiments *UKAEA Harwell Technical Report* HL74.1054(c13)
Osborn R 1993 private communication
[15] Rainford B D and Adroja D T 1997 to be published
[16] Newman D J and Ng B 1989 *Rep. Prog. Phys.* **52** 699
[17] Peschel I and Fulde P 1970 *Z. Phys.* **238** 99
[18] Fischer K H 1970 *Springer Tracts in Modern Physics* vol 54, ed G Höhler (Berlin: Springer) p 1